energies

MDPI

Article

Modeling and Numerical Simulation of the Inlet Velocity on Oil–Water Two-Phase Vapor Separation Efficiency by the Hydrocyclone

Shuai Zhao [1,2], Jipeng Sun [2], Shuli Wang [2] and Zhihui Sun [1,*]

[1] School of Mines, China University of Mining and Technology, Xuzhou 221116, China; zhaoshuai6074@cumt.edu.cn
[2] Haiwang Hydrocyclone Co., Ltd., Postdoctoral Innovation Research Base, Weihai 264204, China; jipeng.sun@wh-hw.com (J.S.); shuli.wang@wh-hw.com (S.W.)
* Correspondence: zhsun@cumt.edu.cn

Abstract: The density of tar vapor and water vapor produced by coal pyrolysis is different. Different centrifugal forces will be generated when they flow through the hydrocyclone. The water vapor and tar vapor are divided into inner and outer layers. According to this phenomenon, the moisture in the tar can be removed. In this paper, a Eulerian gas–liquid two-phase flow model is established by numerical simulation to study the effect of inlet velocity on the separation effect of a designed hydrocyclone (split ratio 0.2). The results show that the inlet velocity and moisture content have an influence on the volume distribution characteristics, tangential velocity, axial velocity, pressure drop distribution, and separation efficiency of tar vapor and water vapor in the hydrocyclone. When the inlet velocity increases from 2.0 to 12.0 m/s, the central swirl intensity increases, and the negative pressure sweep range at the overflow outlet increases. The axial velocity increased from 2.8 to 14.9 m/s, tar vapor content at the overflow outlet decreased from 74% to 37%, and at the underflow outlet increased from 89% to 92%. When the moisture content is lower than 10%, the hydrocyclone with the split ratio of 0.20 is no longer suitable for the separation of oil–water two-phase vapor. However, when the water content is higher than 20%, the purity of tar vapor at the underflow outlet can reach 92%, and the overflow outlet needs multistage separation to realize tar purification.

Keywords: pressure-controlled pyrolysis; oil–water separation; centrifugal force; two-phase vapor separation; cyclone separation

Citation: Zhao, S.; Sun, J.; Wang, S.; Sun, Z. Modeling and Numerical Simulation of the Inlet Velocity on Oil–Water Two-Phase Vapor Separation Efficiency by the Hydrocyclone. *Energies* **2022**, *15*, 4900. https://doi.org/10.3390/en15134900

Academic Editors: Gan Feng, Qingxiang Meng, Gan Li and Fei Wu

Received: 30 May 2022
Accepted: 30 June 2022
Published: 4 July 2022

1. Introduction

Rich coal and less oil are the typical features of the Chinese energy structure. In recent years, the rising dependence on foreign crude oil has stimulated the progress of tar extraction from coal [1]. The pressure-controlled pyrolysis technology can extract tar from the abundant coal resources, and obtain important chemical raw materials, such as anthracene, naphthalene, benzene, and toluene. It is not only an important support in the field of the national energy and chemical industry [2,3], but also an important direction of coal classified utilization [4]. For a long time, the research on direct coal liquefaction has focused on the improvement of the catalytic hydrogenation process and equipment [5,6], catalyst selection and preparation [7,8], tar composition, and content optimization [9–11]. However, the water content of tar after coal pyrolysis reaches 10~30% and contains more sulfur ion and chloride ion salts. The presence of water leads to ion ionization and accelerates the corrosion of equipment.

When the temperature decreases, the viscosity of the tar will increase, and the tar will gradually become a non-Newtonian fluid, or even consolidate, which will bring difficulties to the oil–water separation process. The researchers tried to separate tar and water by different methods, such as sedimentation [12], centrifugation [13], heating [14],

infiltration [15], and demulsification [16]. Gai et al. proposed the method of oil–water separation during coal pyrolysis by tar distillation decomposition. When the boiling point of the fraction is 120~140 °C and the volume ratio of the oil–water system is 1:4 at room temperature, the oil content of water can be reduced to less than 300 mg L^{-1} [17], but this method is greatly affected by temperature and is only suitable for less oil content. Li et al. established the kinetic model by using Smoluchowski aggregation theory and Stokes Einstein collision theory. Based on the heating and demulsification dehydration process, they predicted the effects of temperature, viscosity, time, and water content on tar dehydration efficiency [18]. Zelenskiy et al. proposed adding a demulsifier in the tar and water system to strengthen the process of gravity sedimentation, to separate the water in tar. The results show that the water content is reduced from 8~15% to 2~4% [19]. Although this process can remove most of the water from the tar, the demulsifier will dissolve in the tar and cause the secondary pollution.

To sum up, it is necessary to consider a high-speed and efficient separation device to realize the industrial process of oil–water separation. The cyclone separator is an efficient separation device based on medium density, which is widely used in the field of the petroleum and chemical industry. Wang et al., based on the Reynolds stress model (RSM) of the computational fluid dynamics (CFD) software, simulated the de-oiling effect of hydrocyclone with four different single-inlet structures. Within this research, the separation efficiency of the helical inlet hydrocyclone is the most ideal [20]. Sattar et al. thought that it took too long for electrical resistance tomography to generate fault maps, and proposed a new strategy based on the physics and simple logic behind the measurement to monitor the separation in the inline cyclone separator. The results show that the new algorithm is 104 times faster than the electrical resistance tomography in the case of inline eddy current separation [21]. Sattar et al. studied the influence of inlet conditions on the shape and size of the gas core in an inline swirl separator and proposed that the gas core diameter should be measured with the smallest possible invasion to predict the separation behavior and control the process in the best way [22]. The numerical modeling method can eliminate the influence of intrusion behavior on the performance of the hydrocyclone and obtain the strength and shape of the central swirl. Hanane et al. proposed a hybrid IBM-LES method and applied it to simulate laminar pipe flow for the first time. The results show that the method can control the fluid–solid interaction and converge to the exact solution with second-order accuracy [23]. Liu et al. designed a particle size reconstituted hydrocyclone and studied the effects of split ratio and oil content on the separation performance. The results show that the particle size reconstituted hydrocyclone can realize the separation of crude oil and water [24]. Jia et al. used the CFD–PBM numerical simulation method to study the separation mechanism of the hydrocyclone from different scales and showed that the oil–water separation effect was better when the split ratio was 0.2 [25].

After the low-rank coal was pyrolyzed by the pressure-controlled technology, the products flowed out of the high-temperature fluidized bed. At that time, the light fraction, water, and pyrolysis gas are all in the form of high-temperature vapor, with low viscosity and strong rheological characteristics. In this process, the light fraction and water are atomized at high temperature and have different densities. The cyclone separation process can be used to remove the water in the tar according to the difference of centrifugal force caused by the different density of light fractions and water vapor. In this paper, the effect of the hydrocyclone on separating oil–water two-phase vapor is studied by modeling and numerical simulation. According to the previous research results, the overflow split ratio of the hydrocyclone was selected as 0.2. The influence of inlet flow velocity on the stratification property of oil–water two-phase vapor flowing into the hydrocyclone under different water cut conditions is analyzed. The flow field distribution characteristics, phase distribution law, and pressure distribution characteristics of oil–water two-phase vapor in the hydrocyclone are explored, and the separation efficiency of the hydrocyclone with different inlet flow velocity and water content is revealed. This study aims to analyze the influence of process parameters on the separation efficiency of the finalized hydrocyclone, optimize the inlet

flow corresponding to different water contents, and improve the separation efficiency of two-phase vapor, to optimize the structure of the hydrocyclone, promote the application field of the hydrocyclone, and provide guidance and help for the hydrocyclone separation technology of oil–water two-phase vapor.

2. Establish the Numerical Model

2.1. The Operation Process

The pressure-controlled pyrolysis process of low-rank coal was carried out with nitrogen as the protection and displacement medium, as shown in Figure 1. Nitrogen was input to the booster through the pressure relief valve. After the pressurization process is completed, it was stored in the air storage tank at the bottom of the booster. The pyrolysis process of low-rank coal was completed in a fluidized bed. High-pressure nitrogen was used to purge the fluidized bed, and the pyrolysis gas, tar vapor, and water vapor were purged into the cyclone separator to complete the oil–water separation process.

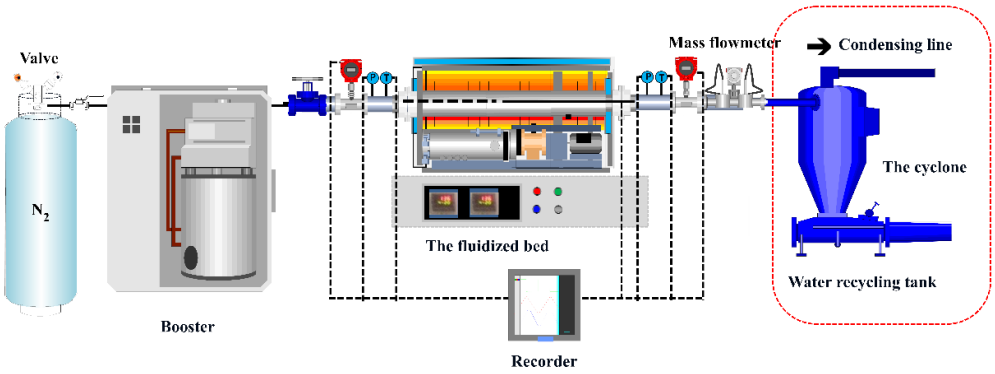

Figure 1. Low-rank coal pyrolysis and product separation system.

2.2. Geometric Model

The tangential inlet single-cone cyclone model was selected, and the structural parameters are shown in Table 1.

Table 1. The structural parameters of the cyclone.

Attribute	Symbol	Value	Unit
Inlet cross-sectional area	A_1	453.00	mm^2
Overflow pipe diameter	D_1	10.70	mm
Length of overflow pipe	L_1	25.00	mm
Depth of overflow pipe	H_1	12.50	mm
Spacing between overflow pipe and swirl chamber	L_2	6.25	mm
Swirl chamber diameter	D_2	60.00	mm
Swirl chamber height	H_2	75.00	mm
Cone length	L_3	276	mm
Cone angle	α	11.75	°
Underflow outlet diameter	D_3	12.5	mm

The fluent preprocessor was used to divide the hexahedral mesh, as shown in Figure 2. The grid cell size was 1.0 mm, and grid encryption was carried out at joints, corners, entrances, and exits [26]. The pressure loss along the way was selected for grid independence verification. The number of grids was 327,742, 237,682, and 124,578, respectively, and the pressure drop was 0.182, 0.176, and 0.137 kPa, respectively. In this paper, the model with 237,682 grids was selected to complete the simulation. The type of boundary layer was defined as no slip boundary, and the thickness was 1.0 mm.

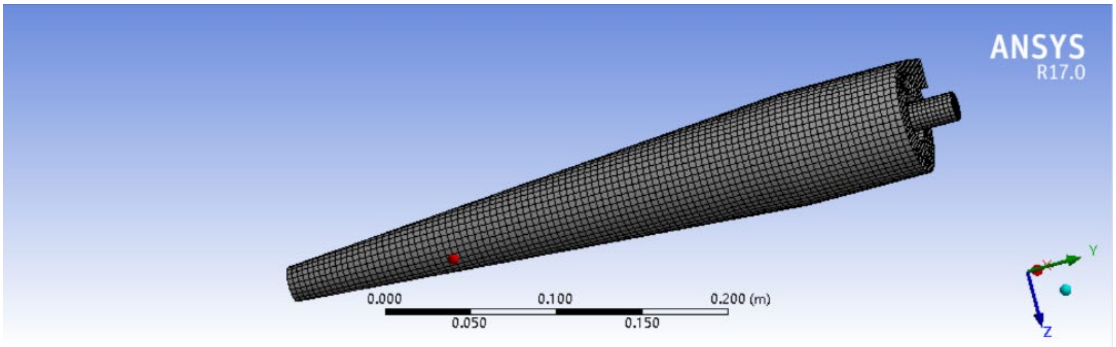

Figure 2. Grid division of the cyclone.

2.3. Governing Equations

The volume distribution, turbulence intensity, tangential velocity, and axial velocity of tar vapor and water vapor in the hydrocyclone follow the conservation law of mass and energy. The moisture content was between 10% and 30%, which meets the selection characteristics of a dispersed phase volume ratio exceeding 10%. Therefore, the Euler method was selected for fluid analysis of oil–water two-phase vapor. The parameter characteristics are shown in Table 2.

Table 2. The characteristic parameters of oil–water two-phase vapor.

Attribute	Symbol	Value	Unit
Tar vapor density	ρ_1	4.84	kg/m^3
Tar vapor heat transfer coefficient	k_1	0.0178	$W/m^2 \cdot K$
Tar vapor viscosity	μ_1	6.75×10^{-6}	$N \cdot s/m^2$
Water vapor density	ρ_2	0.5542	kg/m^3
Water vapor heat transfer coefficient	k_2	0.0261	$W/m^2 \cdot K$
Water vapor viscosity	μ_2	1.34×10^{-5}	$N \cdot s/m^2$
Convection term C_1	C_1	1.44	-
Convection term C_2	C_2	1.92	-
Tar vapor particle size	d	0.0004	m
Moisture content		10%; 20%; 30%; 40%	-
Inlet velocity	u	2; 4; 8; 12	m/s

The separation process of two-phase vapor in the cyclone presented an internal and external two-layer swirl; especially, the turbulence degree of the internal swirl was higher, and the anisotropy was more obvious [27,28]. The Reynolds stress model (RSM) considers the characteristics of rapid change of vortex, rotation, and tension in engineering turbulence calculation, and can solve the problem of anisotropy of the internal and external vortex [29].

Transport equation of each component in RSM:

$$\frac{\partial\left(\rho\overline{u_i'u_j'}\right)}{\partial t} + \frac{\partial\left(\rho u_k\overline{u_i'u_j'}\right)}{\partial x_k} = \frac{D\left(\rho\overline{u_i'u_j'}\right)}{Dt} = D_{i,j} + P_{i,j} + G_{i,j} + \Phi_{i,j} - \varepsilon_{i,j} + F_{i,j}$$

where $D_{i,j}$—the diffusion term of the turbulence model, $P_{i,j}$—the shear stress generation term, $G_{i,j}$—the buoyancy generation term, $\varphi_{i,j}$—pressure strain redistribution, $\varepsilon_{i,j}$—the viscous dissipation term, and $F_{i,j}$—the rotation generation term of two-phase system.

$$D_{i,j} = -\frac{\partial}{\partial t}\left[\rho\overline{u_i'u_j'u_k'} + \overline{P\left(\delta_{kj}u_i' + \delta_{ik}u_j'\right)} - \mu\frac{\partial}{\partial x_k}\left(\overline{u_i'u_j'}\right)\right]$$

$$D_{i,j} = -\frac{\partial}{\partial t}\left[\rho\overline{u_i'u_j'u_k'} + \overline{P\left(\delta_{kj}u_i' + \delta_{ik}u_j'\right)} - \mu\frac{\partial}{\partial x_k}\left(\overline{u_i'u_j'}\right)\right]$$

$$P_{i,j} = -\rho\left(\overline{u_i'u_k'}\frac{\partial\overline{u_j'}}{\partial x_k} + \overline{u_j'u_k'}\frac{\partial\overline{u_i'}}{\partial x_k}\right)$$

$$G_{i,j} = -\rho\beta\left(g_i\overline{u_j'\theta} + g_j\overline{u_i'\theta}\right)$$

$$\Phi_{i,j} = \overline{P\left(\frac{\partial u_j'}{\partial x_i} + \frac{\partial u_i'}{\partial x_j}\right)}$$

$$\varepsilon_{i,j} = 2\mu\overline{\frac{\partial u_i'\partial u_j'}{\partial x_k\partial x_k}}$$

$$F_{i,j} = -2\rho\Omega_x\left(\overline{u_j'u_m'}\varepsilon_{ikm} + \overline{u_i'u_m'}\varepsilon_{jkm}\right)$$

where β—coefficient of thermal expansion, m/K, Ω—vortex vector, θ—cone angle of cyclone, °, and g—gravitational acceleration, −9.81 m/s^2.

After calculation and simplification, the final RSM transport equation is as follows:

$$\frac{\partial\left(\rho\overline{u_i'u_j'}\right)}{\partial t} + \frac{\partial\left(\rho u_k\overline{u_i'u_j'}\right)}{\partial x_k} = \frac{\partial}{\partial x_k}\left(\frac{\mu_i}{\delta_{ik}}\overline{\frac{\partial u_i'u_j'}{\partial x_k}} + \mu\overline{\frac{\partial u_i'u_j'}{\partial x_k}}\right) - \rho\left(\overline{u_i'u_k'}\frac{\partial u_j}{\partial x_k} + \overline{u_j'u_k'}\frac{\partial u_i}{\partial x_k}\right) - C_1\rho\frac{\varepsilon}{k}\left(\overline{u_iu_j} - \frac{2}{3}k\delta_{i,j}\right) - C_2\left(P_{i,j} - \frac{1}{3}P_{kk}\delta_{i,j}\right) - \frac{2}{3}\rho\varepsilon\delta_{i,j}$$

where ρ—density, kg/m^3, P—pressure, Pa, K—thermal conductivity, W/(m^2·K), μ—Hydro dynamic viscosity, (N·s)/m^2, u_i—velocity vector, and C_1,C_2—convection coefficients of the k–ε equation.

3. Results and Discussion

3.1. Velocity Distribution

Velocity is an important factor affecting the separation efficiency of the cyclone, especially the tangential velocity, which determines the centrifugal force [30,31]. As shown in Figure 3, it is the velocity nephogram of tar vapor in the cyclone under different inlet velocities. The flow velocity was large at the overflow outlet, swirl chamber, and cone wall of the cyclone. That is because in the hydrocyclone, two layers of internal and external swirls with opposite directions were formed. The internal swirls are also called the forced vortex zone. The external swirling flow is also called the semi-free vortex zone. When the inlet velocity was 2.0 m/s, the hydrocyclone could not form the swirl or the forced vortex zone. When the inlet velocity was greater than 4.0 m/s, the vortex intensity in the forced vortex zone gradually increased, and the higher the inlet velocity, the smaller the radius of the forced vortex zone and the stronger the suction capacity. The main component of the forced vortex zone is water vapor. The density of water vapor was smaller than that of tar vapor, and the centrifugal force was lower. However, due to the suction of high-speed fluid, the turbulence degree of water vapor was high, so the axial velocity was high. The tangential velocity in the center of the forced vortex zone was almost 0. The main component is tar vapor in the semi-free vortex zone. Due to the high density, the tar vapor also bears high centrifugal force, which leads to the small axial velocity of tar vapor and the large tangential velocity and has the characteristics of wall attachment.

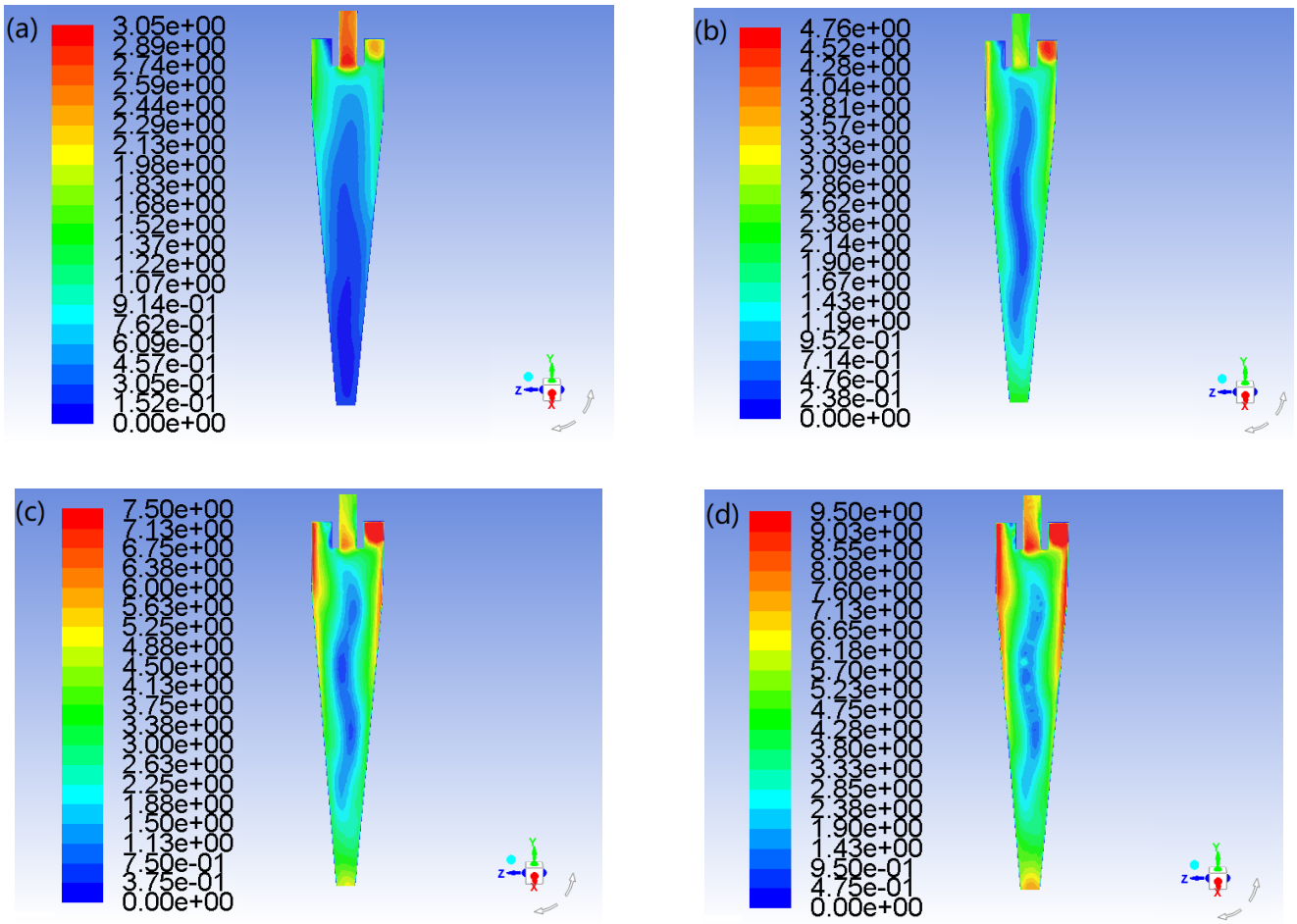

Figure 3. The velocity nephogram of tar vapor under different inlet velocities: (**a**) 2.0 m/s, (**b**) 4.0 m/s, (**c**) 8.0 m/s, and (**d**) 12.0 m/s.

The monitoring curve was set at the conical section and central axis of the cyclone, and the tangential velocity of the cyclone was asymmetrically distributed along the radial direction, as shown in Figure 4a. The flow velocity at the cone section wall was higher and increased with the increase of the inlet flow velocity. This is because when the moisture content is the same, the centrifugal force will increase with the increase of the inlet velocity, and then the tangential velocity will also increase [32]. The influence of the inlet velocity on the axial velocity is mainly reflected in the overflow outlet, as shown in Figure 4b. With the increase of the inlet velocity, the velocity at the underflow outlet and cone section showed little change, while the velocity at the overflow outlet increased a lot. This is because the outflow phase at the underflow outlet was mainly tar vapor with high density, and the flow velocity of tar vapor along the cone wall at the edge of the swirl was low. Even if the inlet velocity is increased, the rate of tar vapor wall-attached flow will not greatly increase.

At the same inlet velocity, the moisture content of two−phase vapor had a weak effect on the distribution of tangential and axial velocity. With the increase of moisture content, the tangential velocity decreased a little, while the axial velocity increased a little, as shown in Figure 4c,d. This is because the density of water vapor is lower than that of tar vapor. When the inlet velocity is constant, the increase of light phase content means that the content of tar vapor is relatively reduced. This led to the decrease of the average density of the two-phase system, so the centrifugal force decreased accordingly, and the tangential velocity also decreased. On the other hand, the negative pressure formed by axial swirl had a suction effect on the central fluid. With the increase of water vapor content, the central fluid density decreased relatively, the effect of suction was amplified, and the velocity of

the axial overflow outlet increased. However, the flow velocity at the underflow outlet is mainly the wall-attached flow of tar vapor, so the moisture content had little effect on it.

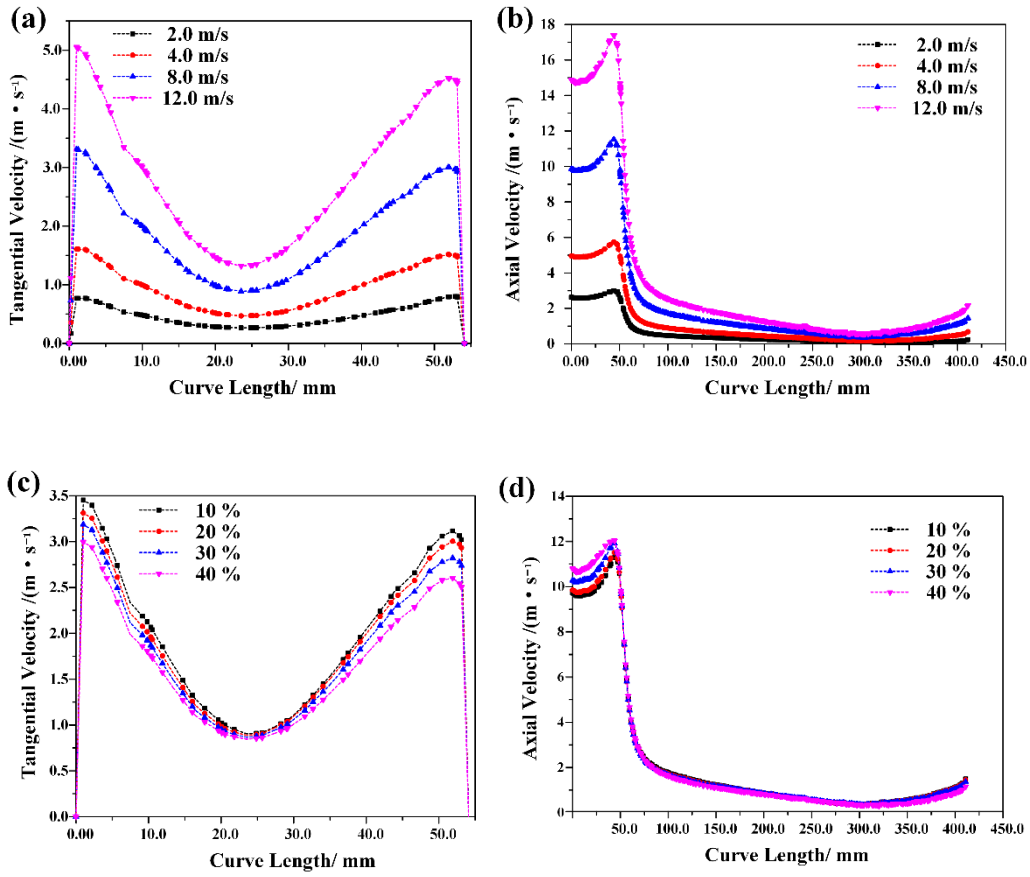

Figure 4. The velocity distribution of tar vapor. (**a**) Tangential velocity with water content of 20%, (**b**) axial velocity with water content of 20%, (**c**) tangential velocity when inlet velocity is 8.0 m/s, and (**d**) axial velocity when inlet velocity is 8.0 m/s.

3.2. The Partial Pressure of Tar Vapor Phase

As shown in Figure 5, when the water vapor content of the two-phase system was 20%, the tar stream and water vapor distribution occurred in the section of the cyclone. When the inlet velocity was 2.0 m/s, the intensity of the axial swirl in the center of the cyclone was low, and the suction effect was not obvious. The water vapor with lower density accumulated in the swirl chamber and flowed out from the overflow outlet, and only a small amount of tar vapor flowed on the wall. When the inlet velocity was higher than 4.0 m/s, the intensity of the central swirl increased and the suction effect on water vapor phase was more obvious. The aggregation degree of tar vapor in the outer swirl increased with the increase of the inlet velocity.

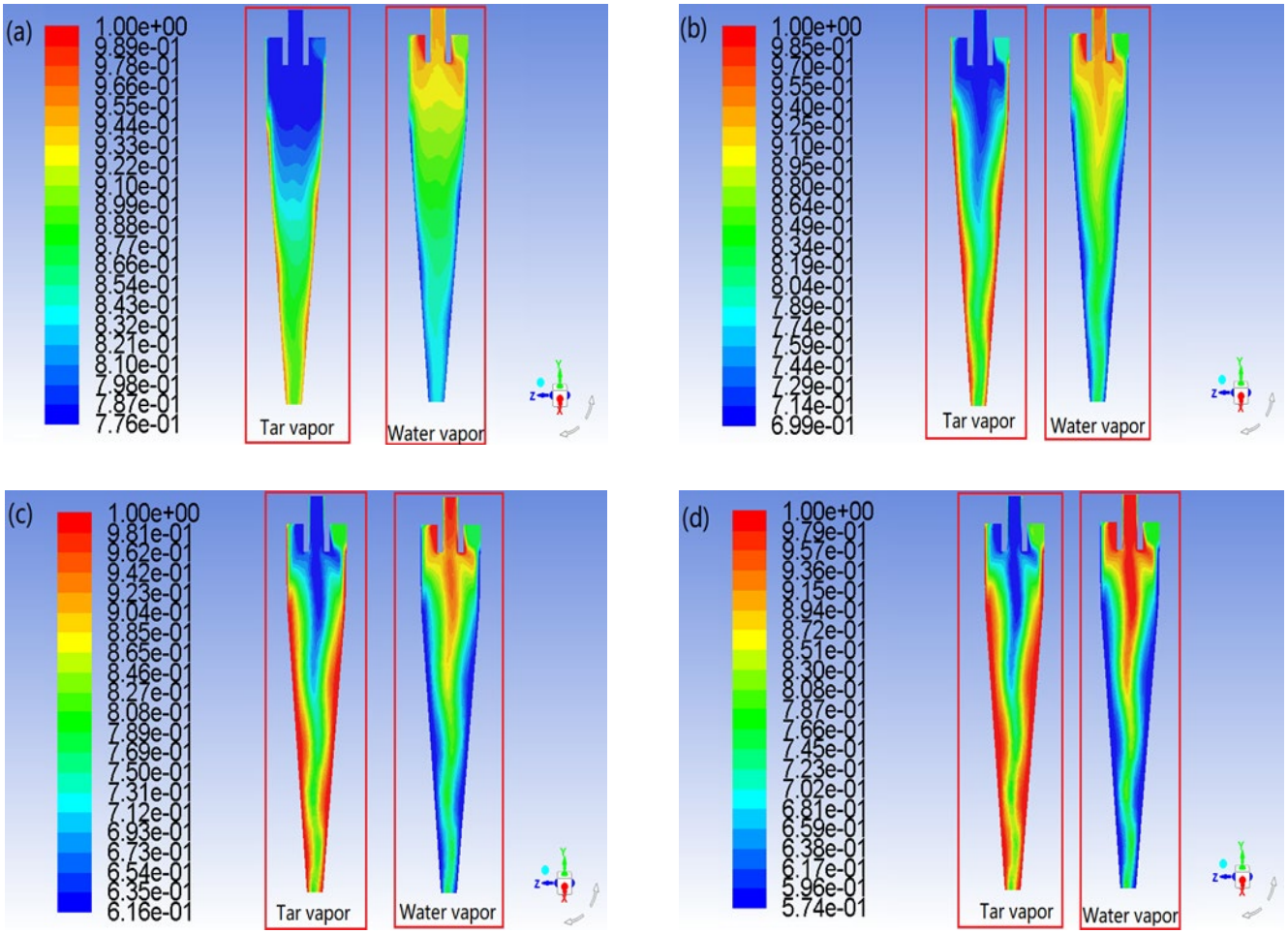

Figure 5. The phase distribution of tar vapor and water vapor in cyclone section with water content of 20%. (**a**) Inlet velocity 2.0 m/s, (**b**) inlet velocity 4.0 m/s, (**c**) inlet velocity 8.0 m/s, and (**d**) inlet velocity 12.0 m/s.

The partial pressure of tar vapor in the radial and axial direction of the cyclone also confirmed the above view. As shown in Figure 6a, when the moisture content of the two-phase system was 20% and the inlet velocity was 2.0 m/s, there was no obvious difference in the radial partial pressure of tar vapor. When the inlet velocity was greater than 4.0 m/s, the partial pressure of tar vapor increased in the radial direction, especially within 10 mm of the cone wall. The partial pressure of tar vapor in the center of the cyclone was low, and this trend was more obvious with the increase of the inlet velocity. When the inlet velocity was 8.0 m/s, as shown in Figure 6b, the content of water vapor also had a weak influence on the partial pressure of tar vapor. With the increase of the water vapor content, the radial partial pressure of tar vapor decreased, especially within 10 mm of the cone wall. This is mainly because the centrifugal force of tar vapor decreased when the inlet velocity was constant. The increased water vapor content led the average density to decrease in the two-phase system. The axial partial pressure of tar vapor in the cyclone also has similar characteristics. As shown in Figure 6c, when the moisture content of the two-phase system was 20% and the inlet velocity was 2.0 m/s, the axial partial pressure of tar vapor was only slightly different at the overflow outlet, swirl chamber, and cone section. With the increase of the inlet velocity, the partial pressure of tar vapor at the swirl chamber and cone section increased, and the partial pressure of tar vapor at the overflow outlet was almost without any change. The contact position between the overflow pipe and the swirl chamber presented negative pressure, which was caused by the suction effect of the axial swirl. This

is beneficial to increase the axial velocity, reduce the tangential velocity in the center of the cyclone, and improve the separation efficiency. In addition, with the increase of the water vapor content, as shown in Figure 6d, there was no significant difference of pressure in the overflow outlet when the inlet velocity was 8.0 m/s. The pressure of the swirl chamber and the cone section showed a decreasing trend. Combined with the nephogram of tar vapor distribution, the increase of water vapor content led to the increase of the central cyclone degree, so the centrifugal force of tar vapor increased, and the content in the center of the cyclone decreased.

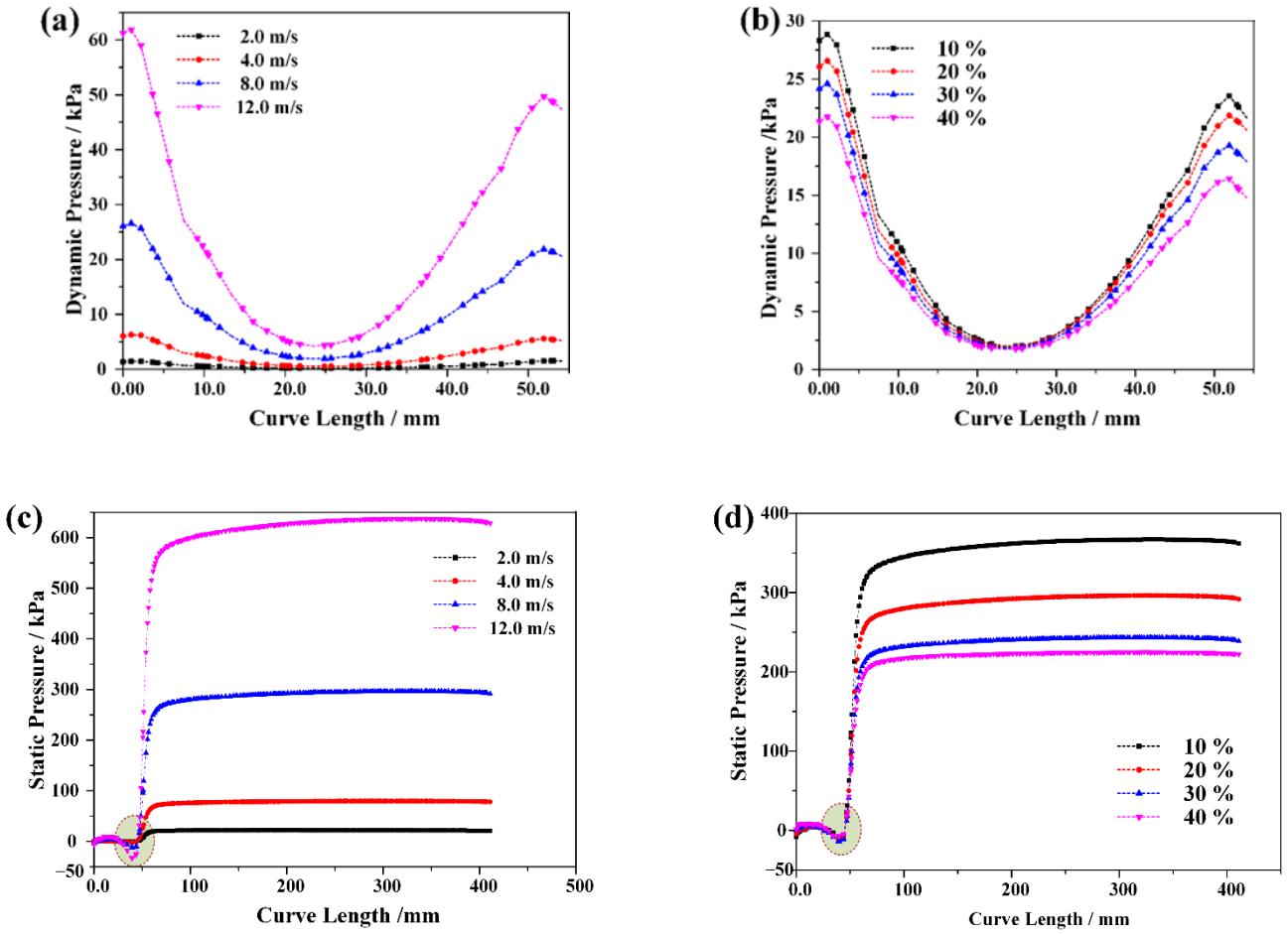

Figure 6. The partial pressure of tar vapor in radial and axial direction of cyclone. (**a**) Radial pressure with water content of 20%, (**b**) radial pressure when inlet velocity is 8.0 m/s, (**c**) axial pressure with water content of 20%, and (**d**) axial pressure when inlet velocity is 8.0 m/s.

3.3. Volume Distribution Characteristics of Tar Vapor

The streamline distribution characteristics of water vapor flowing in the cyclone are shown in Figure 7a, b. The density of water vapor was smaller than that of tar vapor, which was mainly distributed in the upper layer of the cyclone and flowed out through the overflow outlet. When the inlet velocity was within the range of 2.0~12.0 m/s, the flow area of water vapor was greatly affected by the inlet velocity. When the inlet velocity was 4.0 m/s, the water vapor flow area was in the upper part of the swirl chamber and the cone section. With the increase of inlet velocity, the entrainment of the internal swirl formed in the center of the cyclone was strengthened, and the occupied volume of water vapor in the swirl chamber was gradually reduced.

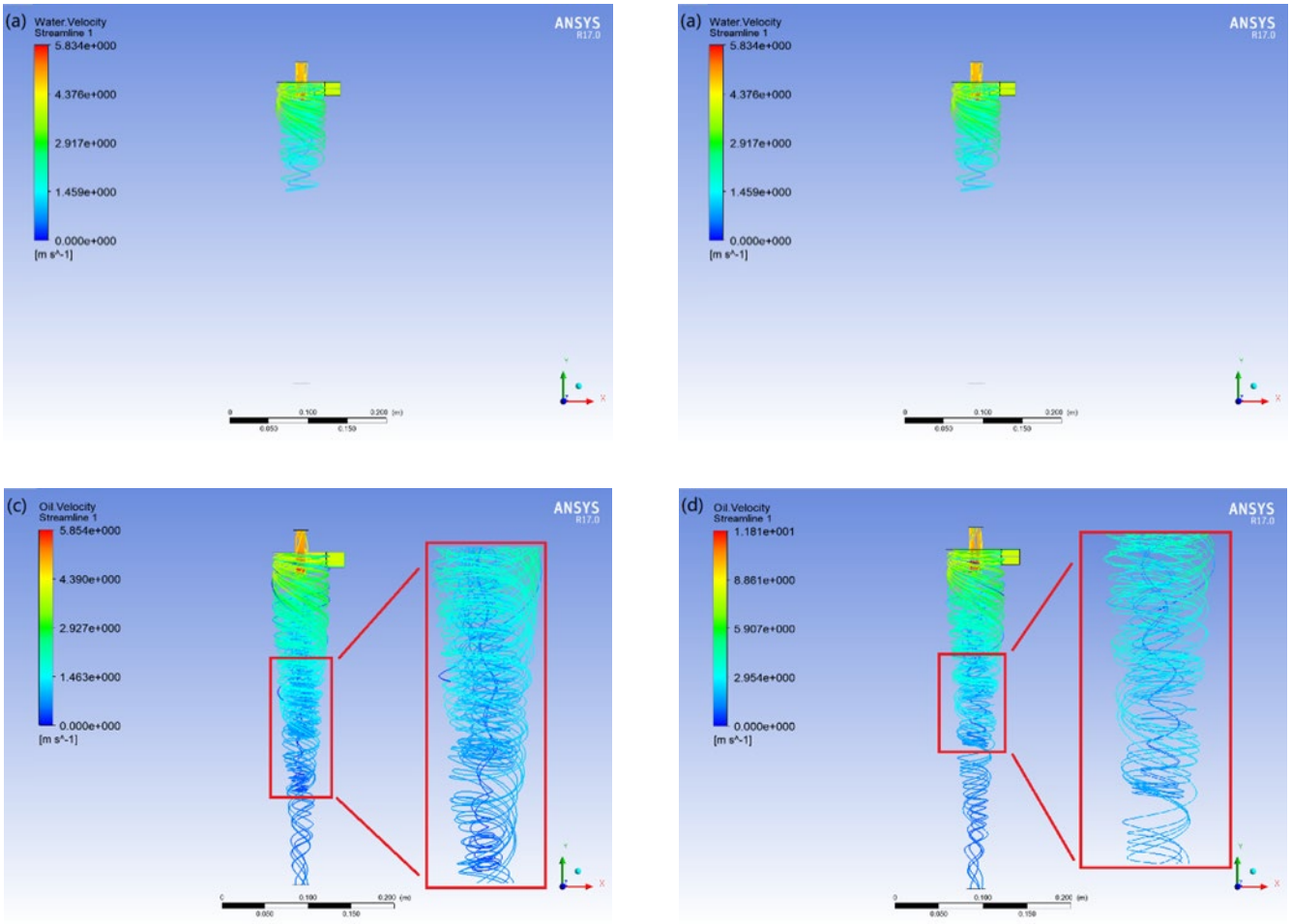

Figure 7. The streamline distribution of water vapor and tar vapor in cyclone. (**a**) Water vapor streamline when inlet velocity is 4.0 m/s, (**b**) water vapor streamline when inlet velocity is 8.0 m/s, (**c**) tar vapor streamline when inlet velocity is 4.0 m/s, and (**d**) tar vapor streamline when inlet velocity is 8.0 m/s.

The tar vapor with high density mainly flows out from the underflow outlet of the cyclone, but some tar vapor will still flow out from the overflow outlet due to the entrainment of the internal cyclone. With the increase of inlet velocity, the centrifugal force on tar vapor increased, so the entrainment effect of the central swirl on tar vapor gradually decreased, as shown in Figure 7c,d. The distribution of the tar vapor flow line in the internal swirl gradually decreased with the increase of the inlet velocity. This is mainly because the increase of the inlet velocity led to the increase of tangential velocity of the two-phase vapor in the swirl chamber. The centrifugal force of tar vapor was further increased, and more tar vapor was thrown to the outside of the swirl, and then flowed, attached to the wall [33].

The volume distribution of tar vapor in the radial direction of the cyclone is shown in Figure 8. The inlet velocity and moisture content had significant effects on the distribution of tar vapor. The tar vapor with a content greater than 85% was mainly distributed within 10 mm of the outer swirl. When the moisture content was 20%, as shown in Figure 8a, the content of tar vapor in the central swirl was 67~83%. With the increase of inlet velocity, the tar vapor content of the central swirl decreased, and the tar vapor content gradually increased within 10 mm to the wall. When the inlet velocity was 8.0 m/s, as shown in Figure 8b, with the increase of moisture content, the volume fraction difference of the tar vapor between the outside and the center of the swirl increased, which is more conducive to the separation of the two-phase vapor.

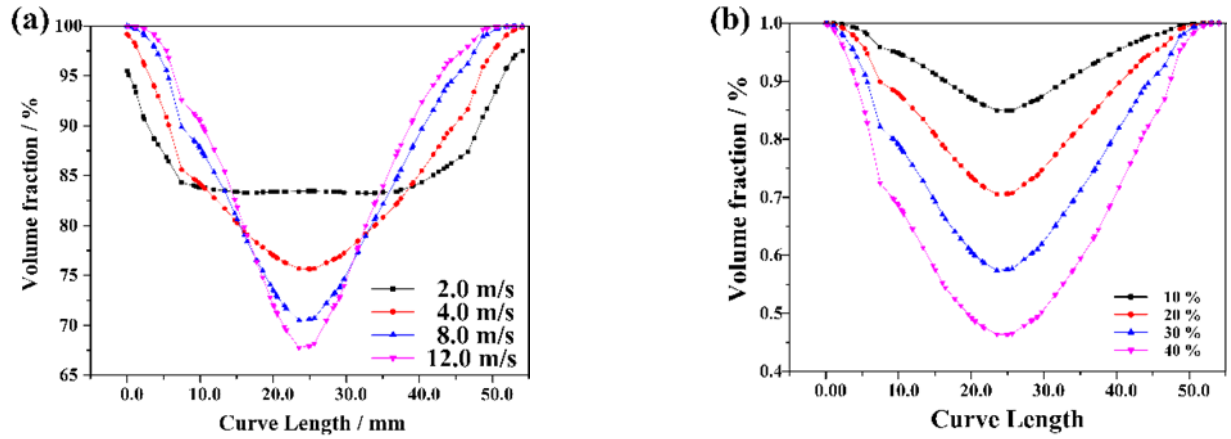

Figure 8. Volume distribution characteristics of tar vapor in the radial direction of the cyclone. (**a**) The water content is 20% and (**b**) the inlet velocity is 8.0 m/s.

The axial distribution difference of tar vapor is mainly reflected in the volume fraction flowing out from overflow and underflow outlet. As shown in Figure 9a, when the moisture content was 20%, the volume fraction of tar vapor at the overflow outlet was about 70~86.43%, and the volume fraction at the underflow outlet was 92.07%. The increase of inlet velocity will reduce the volume fraction of tar vapor at the overflow outlet, but it had little effect on the volume fraction of tar vapor at the underflow outlet. When the inlet velocity was 8.0 m/s and the moisture content was 10%, as shown in Figure 9b, the volume fraction of tar vapor at the overflow outlet was 74.69%. Under the condition of constant inlet velocity, with the increase of moisture content, the volume fraction of tar vapor at the overflow outlet gradually decreased to 37.54%; however, at the underflow outlet, it was almost unaffected, about 90%.

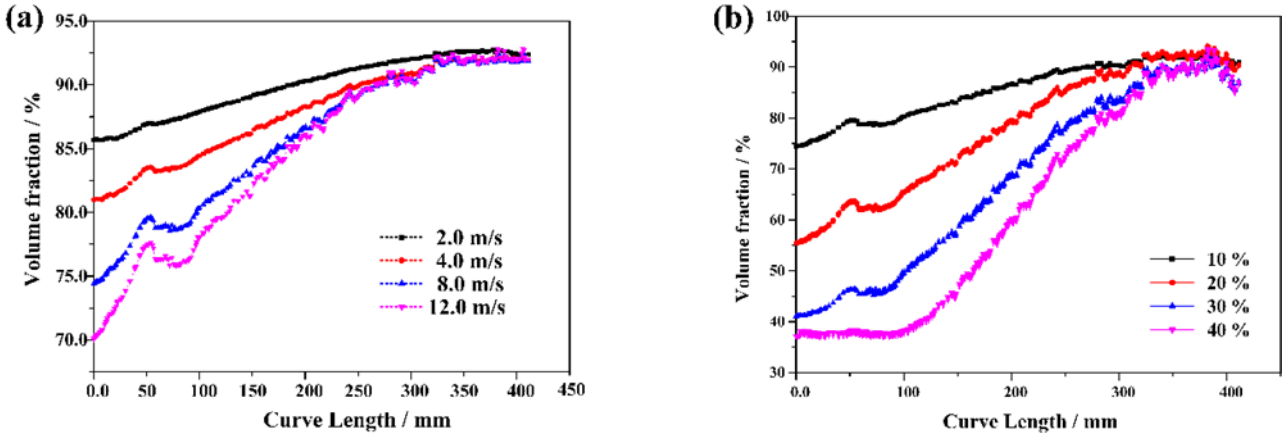

Figure 9. Volume distribution characteristics of tar vapor in the axial direction of the cyclone. (**a**) The water content is 20% and (**b**) the inlet velocity is 8.0 m/s.

The separation efficiency of the two-phase vapor is an important parameter to measure the working performance of the cyclone. As shown in Figure 10a, when the moisture content was 20%, the influence of inlet velocity on the separation efficiency of the cyclone was mainly reflected in the volume fraction of tar vapor at the overflow outlet. When the inlet velocity increased from 2.0 to 12.0 m/s, the volume fraction of tar vapor at the overflow outlet decreased from 74.27% to 47.76%, while the tar vapor volume fraction at the underflow outlet changed slightly, from 89.02% to 94.04%. In addition, the moisture content of the two-phase system also affects the separation efficiency of the cyclone, as shown in Figure 10b. When the inlet velocity was 8.0 m/s and the moisture content increased

from 10% to 40%, the content of tar vapor at the overflow outlet decreased from 75.04% to 37.56%, and at the underflow outlet it decreased from 97.41% to 92.34%. The cyclone is not suitable for oil–water separation when the moisture content of the two-phase system is less than 10%. When the moisture content is higher than 20%, the two-phase system flowing out from the overflow outlet shall adopt the form of multi-stage cyclone combination to separate the oil–water of the two-phase vapor again.

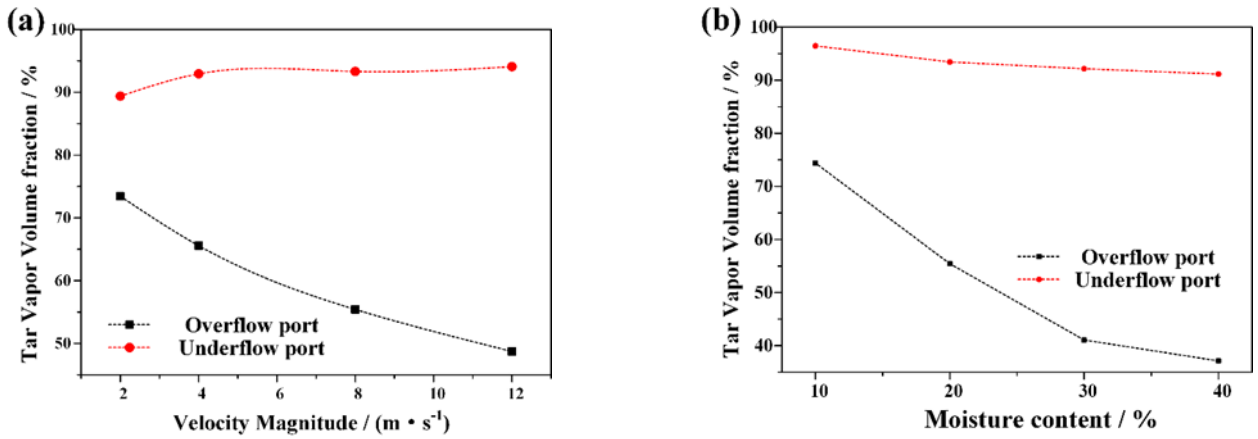

Figure 10. The separation efficiency of the cyclone. (**a**) At the overflow outlet and (**b**) at the underflow outlet.

4. Conclusions

In this paper, the effect of inlet velocity on the separation efficiency of the designed hydrocyclone was studied by numerical simulation. A Eulerian gas–liquid two-phase flow model was established to investigate the variation trend of inlet velocity and moisture content on the volume distribution characteristics, radial pressure drop, tangential velocity, and axial velocity of tar vapor and water vapor in the designed hydrocyclone, with a split ratio of 0.2. When the water content was 20%, the inlet velocity increased from 2.0 to 12.0 m/s, and the separation efficiency of the cyclone also increased from 89.02% to 94.04%. However, the increase of water content will reduce the radial pressure gradient of the hydrocyclone, weaken the turbulence degree in the forced vortex area of the hydrocyclone, and then reduce the stratification effect. On the other hand, when the moisture content of the two-phase system was less than 10%, the cyclone was not suitable for oil–water separation. When the moisture content was higher than 20%, the two-phase system flowing out from the overflow outlet shall adopt the form of multistage cyclone combination to separate the oil–water of the two-phase vapor again.

Author Contributions: Formal analysis, writing—original draft preparation, S.Z.; writing—review and editing, Z.S., methodology, project administration, J.S. and S.W. All authors have read and agreed to the published version of the manuscript.

Funding: This research was funded by "Jiangsu Natural Science Youth Fund grant number BK20221133", "The Fundamental Research Funds for the Central Universities, grant number 2021QN1002", "China Postdoctoral Science Foundation, grant number 2021M693421", and "The 2021 Jiangsu Shuang chuang (Mass Innovation and Entrepreneurship) Talent Program, grant number JSSCBS20211238".

Acknowledgments: This study was supported by "Jiangsu Natural Science Youth Fund, grant number BK20221133", "The Fundamental Research Funds for the Central Universities, grant number 2021QN1002", "China Postdoctoral Science Foundation, grant number 2021M693421", and "The 2021 Jiangsu Shuangchuang (Mass Innovation and Entrepreneurship) Talent Program, grant number JSSCBS20211238". The authors also express their appreciation to the technical reviewers for their constructive comments.

Conflicts of Interest: The authors declare no conflict of interest.

References

1. Wu, Q.; Tu, K.; Zeng, Y.F.; Liu, S.Q. Discussion on the main problems and countermeasures for building an upgrade version of main energy (coal) industry in China. *J. China Coal Soc.* **2019**, *44*, 1625–1636.
2. Zou, C.; Chen, Y.; Kong, L.; Sun, F.; Shanshan, C.; Zhen, D. Underground coal gasification and its strategic significance to the development of natural gas industry in China. *Pet. Explor. Dev.* **2019**, *46*, 195–204. [CrossRef]
3. Yang, J.X.; Wei, W.J.; Qi, Y. Research progress on hyper-coal for efficient utilization. *J. China Coal Soc.* **2020**, *9*, 3301–3313.
4. Li, J.; Mao, X.; Zhong, J.; Liu, M. Carbon Nanotubes Catalyst Modified via NiMoP and Its Performance in the Hydrogenation of Direct Coal Liquefaction Oil. *Acta Pet. Sin.* **2019**, *35*, 1167–1174.
5. Liu, M.; Chen, G.F.; Wang, Y.G.; Zhao, P.; Qu, S.J. Conversion of sulphur and nitrogen compounds in hydrofining process of Baishihu coal liquefaction oil. *J. Fuel Chem. Technol.* **2019**, *47*, 870–875.
6. Liu, L.; Zhao, L.; Sun, Y.; Gao, S.; Jiang, M.; Jiang, M.; Rosso, D. Separation performance of hydrocyclones with medium rearrangement internals. *J. Environ. Chem. Eng.* **2021**, *9*, 105642. [CrossRef]
7. Shuai, Z.; Xiaoshu, L.; Qiang, L.; Youhong, S. Thermal-fluid coupling analysis of oil shale pyrolysis and displacement by heat-carrying supercritical carbon dioxide. *Chem. Eng. J.* **2020**, *394*, 125037. [CrossRef]
8. Tong, D.; Zhang, Q.; Liu, F.; Geng, G.; Zheng, Y.; Xue, T.; Hong, C.; Wu, R.; Qin, Y.; He, K. Current Emissions and Future Mitigation Pathways of Coal-Fired Power Plants in China from 2010 to 2030. *Environ. Sci. Technol.* **2018**, *52*, 12905–12914. [CrossRef]
9. Apicella, B.; Russo, C.; Cerciello, F.; Stanzione, F.; Ciajolo, A.; Scherer, V.; Senneca, O. Insights on the role of primary and secondary tar reactions in soot inception during fast pyrolysis of coal. *Fuel* **2020**, *275*, 11795. [CrossRef]
10. Huang, X.; Cheng, D.G.; Chen, F.; Zhan, X. The decomposition of aromatic hydrocarbons during coal pyrolysis in hydrogen plasma: A density functional theory study. *Int. J. Hydrog. Energy* **2012**, *37*, 18040–18049. [CrossRef]
11. Feng, J.; Xue, X.; Li, X.; Li, W.; Guo, X.; Liu, K. Products analysis of Shendong long-flame coal hydropyrolysis with iron-based catalysts. *Fuel Process. Technol.* **2015**, *130*, 96–100. [CrossRef]
12. Tian, Y.; Feng, J.; Cai, Z.; Chao, J.; Zhang, D.; Cui, Y.; Chen, F. Dodecyl Mercaptan Functionalized Copper Mesh for Water Repellence and Oil-water Separation. *J. Bionic Eng.* **2021**, *18*, 887–899. [CrossRef]
13. Zhang, X.; Liu, C.; Yang, J.; Huang, X.J.; Xu, Z.K. Wettability Switchable Membranes for Separating Both Oil-in-water and water-in-oil emulsions. *J. Membr. Sci.* **2021**, *624*, 118976. [CrossRef]
14. Hafsi, Z.; Elaoud, S.; Mishra, M.; Wada, I. Numerical Study of Droplets Coalescence in an Oil-Water Separator. In Proceedings of the International Conference on Advances in Mechanical Engineering and Mechanics; Springer: Cham, Switzerland, 2021; pp. 449–454.
15. Kovaleva, L.; Zinnatullin, R.; Musin, A.; Gabdrafikov, A.; Sultanguzhin, R.; Kireev, V. Influence of radio-frequency and microwave electromagnetic treatment on water-in-oil emulsion separation. *Colloids Surf. A Physicochem. Eng. Asp.* **2021**, *614*, 126081. [CrossRef]
16. Peng, Y.; Yu, B.; Zhang, X.; Gong, H.; Liu, Y. Numerical simulation on the effect of combining centrifugation, electric field and temperature on two-phase separation. *Chem. Eng. Process.* **2020**, *148*, 107803. [CrossRef]
17. Gai, H.; Zhang, X.; Chen, S.; Wang, C.; Xiao, M.; Huang, T.; Wang, J.; Song, H. An improved tar–water separation process of low–rank coal conversion wastewater for increasing the tar yield and reducing the oil content in wastewater. *Chem. Eng. J.* **2020**, *383*, 123229. [CrossRef]
18. Li, H.; Li, D.; Yang, X.; Wang, J.; Li, B.; Li, W.; Zhao, L. Kinetics for dehydration of coal tar. *Chem. Eng. J.* **2011**, *9*, 57–60.
19. Zelenskiy, V.V.; Fillipov, V.L.; Bannikov, L.P.; Karchakova, V.V. Intensifying the separation of water-tar emulsions. *Coke Chem.* **2014**, *57*, 163–166. [CrossRef]
20. Wang, Y.; Zhao, L.; Wang, Y.; Baorui, X.; Minghu, J. Contrastive Analysis on Numerical Simulation of Oil-water Hydrocyclone with Various Inlet Forms. *Fluid Mach.* **2017**, *45*, 22–27.
21. Sattar, M.A.; Garcia, M.M.; Portela, L.M.; Babout, L. A Fast Electrical Resistivity-Based Algorithm to Measure and Visualize Two-Phase Swirling Flows. *Sensors* **2022**, *22*, 1834. [CrossRef]
22. Sattar, M.A.; Garcia, M.M.; Banasiak, R.; Portela, L.M.; Babout, L. Electrical Resistance Tomography for Control Applications: Quantitative Study of the Gas-Liquid Distribution inside A Cyclone. *Sensors* **2020**, *20*, 6069. [CrossRef] [PubMed]
23. Atmani, H.; Zamansky, R.; Climent, E.; Legendre, D. Stochastic wall model for turbulent pipe flow using Immersed Boundary Method and Large Eddy Simulation. *Comput. Fluids* **2022**, *239*, 105419. [CrossRef]
24. Liu, Y.; Ma, J.; He, Y.; Zhao, Y.; Sun, C.; Yin, P.; Zhang, S. Study on the Oil-Water Separation Performance of the Droplet Size Reconstruction Hydrocyclone. *China Pet. Mach.* **2020**, *48*, 90–97.
25. Jia, P.; Chen, J.; Cai, X.; Kong, L.; Wang, C.; Shang, C.; Zhang, M.; Shi, Y. Study on Oil-Water Separation Characteristics of Hydrocyclone Based on CFD-PBM Numerical Simulation. *J. Petrochem. Univ.* **2021**, *34*, 58–65.
26. Nunes, S.A.; Magalhães, H.L.; Gomez, R.S.; Vilela, A.F.; Figueiredo, M.J.; Santos, R.S.; Rolim, F.D.; Souza, R.A.A.; de Farias Neto, S.R.; Lima, A.; et al. Oily Water Separation Process Using Hydrocyclone of Porous Membrane Wall: A Numerical Investigation. *Membranes* **2021**, *11*, 79. [CrossRef]
27. Li, S.; Li, R.; Nicolleau, F.C.; Wang, Z.; Yan, Y.; Xu, Y.; Chen, X. Study on oil–water two-phase flow characteristicsof the hydrocyclone under periodic excitation. *Chem. Eng. Res. Des.* **2020**, *159*, 215–224. [CrossRef]
28. Li, F.; Liu, P.; Yang, X.; Zhang, Y.; Zhao, Y. Effects of inlet concentration on the hydrocyclone separation performance with different inlet velocity. *Powder Technol.* **2020**, *375*, 337–351. [CrossRef]

29. Jing, J.; Zhang, S.; Qin, M.; Luo, J.; Shan, Y.; Cheng, Y.; Tan, J. Numerical simulation study of offshore heavy oil desanding by hydrocyclones. *Sep. Purif. Technol.* **2021**, *258*, 118051. [CrossRef]
30. Lv, W.J.; Dang, Z.H.; He, Y.; Chang, Y.L.; Ma, S.H.; Liu, B.; Gao, L.; Ma, L. UU-type parallel mini-hydrocyclone group for oil-water separation in methanol-to-olefin industrial wastewater. *Chem. Eng. Process. Process Intensif.* **2020**, *149*, 107846. [CrossRef]
31. Liu, L.; Zhao, L.; Yang, X.; Wang, Y.; Xu, B.; Liang, B. Innovative design and study of an oil-water coupling separation magnetic hydrocyclone. *Sep. Purif. Technol.* **2019**, *213*, 389–400. [CrossRef]
32. Yang, M.; Jiang, R.; Wu, X.; Hu, Z.; Yue, Y.; Chen, Y. Numerical analysis of flow field and separation characteristics in an oilfield sewage separation device. *Adv. Powder Technol.* **2021**, *32*, 771–778. [CrossRef]
33. Zeng, X.; Zhao, L.; Zhao, W.; Hou, M.; Zhu, F.; Fan, G.; Yan, C. Experimental Study on a Novel Axial Separator for Oil–Water Separation. *Ind. Eng. Chem. Res.* **2020**, *59*, 21177–21186. [CrossRef]